Honors Thesis

# A COMPARISON OF PTYCHOGRAPHY PROGRAMS FOR LENS-LESS IMAGING WITH A HIGH HARMONIC GENERATION SOURCE

by
Aaron Redd

Submitted to Brigham Young University in partial fulfillment
of graduation requirements for University Honors

Department of Physics and Astronomy
Brigham Young University
April 2024

Advisor: Richard Sandberg

Honors Coordinator: Karine Chesnel

# ABSTRACT

## A COMPARISON OF PTYCHOGRAPHY PROGRAMS FOR LENS-LESS IMAGING WITH A HIGH HARMONIC GENERATION SOURCE

Aaron Redd

Department of Physics and Astronomy

Bachelor of Science

High Harmonic Generation provides a coherent source of extreme ultraviolet photons. Tuned to the correct energies, these photons can probe electronic transitions associated with the magnetic moment of many magnetic materials. This thesis provides an investigation into performing ptychographic imaging with a high harmonic source as a step towards performing high resolution imaging of magnetic domains. Three ptychography codes (Ptychodactyl, PyNX, and Tike), are compared for image reconstruction quality and ease of use. Tike and Ptychodactyl prove more successful than PyNX. These first two programs reconstruct data from a simple helium-neon laser setup with great success, and Tike demonstrates promise with data gathered from the high harmonic generation setup.

# ACKNOWLEDGMENTS

I would like to acknowledge the support and involvement of several graduate students, including Taylor Buckway. I can thank him for building almost all of the High Harmonic Generation system, and for helping me gain experience with ultrafast optics. I would like to thank graduate student Nick Porter for writing the very useful and approachable ptychography code Ptychodactyl–this code was quite useful in this thesis. I'd also like to thank graduate student Daniel Hodge who helped me understand various phase retrieval algorithms, and of course I'd like to thank Richard Sandberg, my research adviser, who made all of this possible. This work was primarily funded through BYU Department of Physics and Astronomy Mentoring Funds.

# Contents

# List of Figures

# Chapter 1

# Introduction

## 1.1 Lens and Lensless imaging

Lenses recreate images of distant objects by performing spatial Fourier transforms. This is possible due to both the fact that the lens material has a different index of refraction than the medium surrounding it (often air), and because the lens material, while refracting the light, still allows most of it through without being absorbed. There are numerous types of lenses available for different wavelengths, but they all depend on the material having these two properties. When it comes to photons spanning from the ultraviolet to the soft x-ray regimes, the materials conventionally used in lenses become highly absorbing to these photons, making such optics useless for imaging at these wavelengths. As shown in the Rayleigh Criterion, shorter wavelengths, such extreme ultraviolet (EUV) and soft x-ray, allow for the imaging of smaller features. This relation is shown in the following equation

$$r = \frac{0.61\lambda}{NA} \tag{1.1}$$

where $r$ is the transverse or spatial resolution, $\lambda$ is the wavelength of light used, $NA$ is the numerical aperture, and the 0.61 is the constant defined by Rayleigh as the minimum

possible value that enables us to distinguish one object from another. This value is somewhat arbitrary, but the relation is irrefutable—the smallest feature a light source can image is directly proportional to the wavelength used, or the shorter the wavelength, the sharper the image [1]. The numerical aperture, *NA*, is described by the equation

$$NA = n\sin\theta \tag{1.2}$$

where $n$ is the index of refraction of the material and $\theta$ is the half angle of the light collected. Due to the simple physics of this equation, scientists use a special methods and equipment in order to image with EUV and x-ray photons.

Scientists working in the x-ray regime often makes use of diffractive (instead of refractive) optics to produce an image. One of the most common examples of this is the Fresnel zone plate, which uses rings of different thicknesses to focus the incident light onto a detector. Other optics for high energy wavelengths consist of grazing incidence mirrors, and multilayer mirrors. Grazing incidence mirrors maximize reflection by keeping the angles between the optic and the mirror surface close to grazing, and are thus best used when the divergence of the incoming light is minimal. multilayer mirrors, however, are usually manufactured to correctly reflect photons that are near normal incidence. While each of these has its place in imaging with high energy photons, they have a number of drawbacks as well, for example, Fresnel zone plates are notoriously difficult to manufacture for shorter wavelengths and even well-made ones produce multiple foci. While the zone plates do focus the beam down, due in part to these multiple foci, they do not act like traditional convex lenses in the visible regime. Because of this, they are most often used upstream from the object to be imaged, providing a more focused beam for probing the sample, instead of being used after the sample to produce an image on the detector.

As hinted to above, grazing incidence optics also suffer from limitations that make them difficult to use after a sample to form an image. As a beam diffracts off a sample its photons

diverge, making all but the most specially engineered of grazing incidence optical setups inefficient at redirecting photons onto a detector to form an image. And finally, for the multilayer mirrors, the issues are two fold: first, the best reflectance for these optics is around 70% [2], with most mirrors performing significantly worse, and second, these mirrors, like the other two types of optics described, are especially sensitive to small variations in the surface of the substrate, and to the variations in the thin films deposited thereupon. Because of these difficulties, scientists often forego the post-sample optics and instead make lensless imaging techniques when using these wavelengths.

Lensless imaging, or more specifically Coherent Diffractive Imaging (CDI), makes use of computer algorithms, along with the sample's diffraction pattern incident on a detector, to reproduce an image of the sample without the use of any optics. As conventional imaging lenses would absorb EUV photons before they had the opportunity to form an image on the detector, these CDI algorithms must in mimic the lens computationally to reproduce the object being imaged. Computers can easily perform the Fourier transform from the a diffraction pattern detected on the Charge-Coupled Device (CCD) to follow the scattered light back to the sample, but in order to do so, it must have both the phase and the intensity of the light incident on the detector. Without the use of interferometry, that phase information is lost, but CDI uses a number of tricks to retrieve that information and reconstruct an image of the sample (see **Fig. 1.1**).

In ordinary CDI, the beam is larger than the sample, and most of the beam passes by it undisturbed [4]. This undisturbed beam interferes with the diffracted beam, and the detected pattern thus preserves the phase information of the diffracted beam. In geometries where the beam is smaller than the sample, it is much more difficult to reconstruct the object. As the CCD detector can only record the intensity (or amplitude squared) of the light that hits it, without some reference beam it can provide only part of the information necessary to

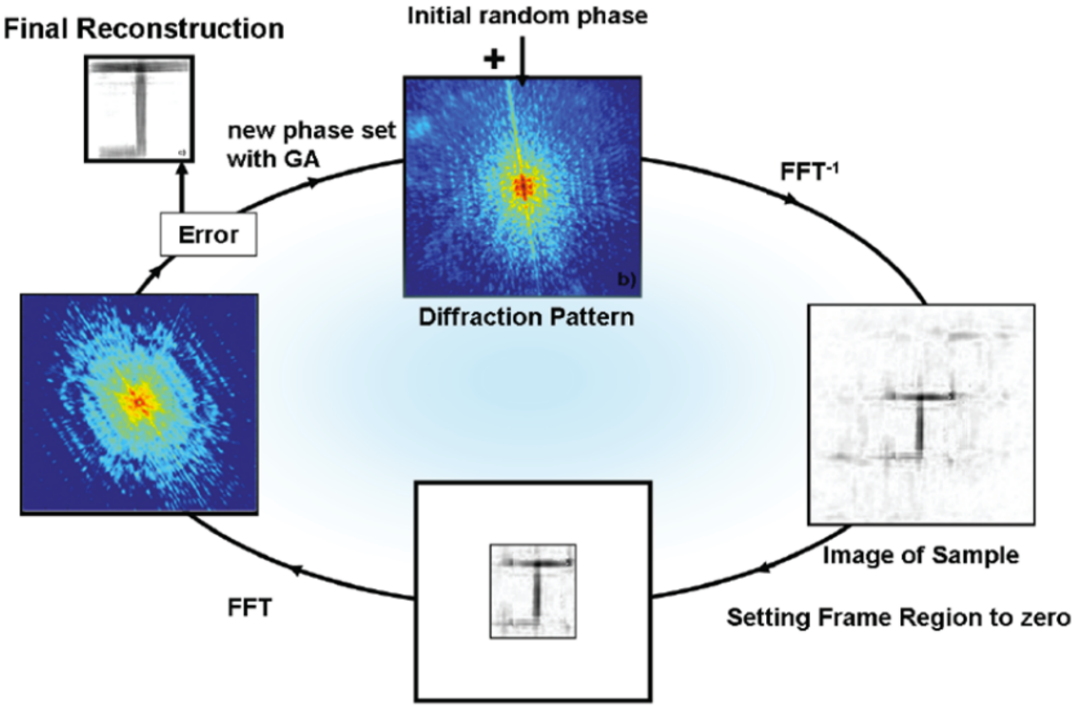


**Figure 1.1** An illustration of iterative phase retrieval. A CCD records a diffraction pattern that contains only the amplitude squared of the light incident upon it, meaning it contains no phase information. After taking the square root of this amplitude matrix to retirieve the intensity of the light incident upon each pixel, it is initialized with a random phase and then back-propagated using an inverse Fast Fourier Transform to retrieve an image of the sample. The random phase produces significant error when back-propagated, some of which can be easily detected and removed with certain constraints. If the sample is known to exist within a specific region, intensity from outside that region can be eliminated. Also, negative intensities can be set to zero. The refined image is then propagated to the Fourier Plane using a forward Fast Fourier Transform, after which the algorithm takes the norm square of the array of values, producing a simulated diffraction pattern. This simulated diffraction pattern will differ from the detected one, so to reduce the error on the next iteration, the amplitude of the simulated diffraction pattern will be replaced with the amplitude obtained from the detected one. Now, with the detected amplitude and the improved guess for the associated phase, the process restarts. Taken from [3].

reconstruct an image. Ptychography is an imaging technique that utilizes many overlapping scans of these extended samples to reconstruct both the probe and the sample. This allows for the reconstruction of samples of infinite size, provided a well-behaved beam and set of translational stages. As with normal CDI, it uses constraints to retrieve the phase and reproduce the sample, but ptychography differs in that some of the constraints are provided by the diffraction patterns from the overlapping regions[6].

## 1.2 Magnetic Imaging and Extreme Ultraviolet Sources

Magnetic materials and effects are increasingly used in a variety of technologies, from electrical motors, powering the future of human travel, to medical Magnetic Resonance Imaging, yielding diagnoses to prolong human life. Many of these technologies, including data storage on hard disk drives, rely on extremely small scale magnetic dynamics, and in order to probe these microscopic dynamics, scientists must use very short wavelengths of light. Additionally, the unpaired electron spins in the Fe atoms can be resonantly probed with photons in the extreme ultraviolet range (52.7 eV or 23.5 nm for the Fe M-edge), and the x-ray ranges (710-740 eV or 1.67-1.75 nm for the Fe L-edge) [5]. Thus, successful magnetic imaging using these transitions requires wavelengths in the EUV and soft x-ray regimes. Traditionally, these magnetic samples have been imaged using tunable light sources such as synchrotrons, which provide highly brilliant and coherent x-ray light of the desired wavelength.

Resonant wavelengths are not the only requirement when attempting magnetic imaging experiments—polarization control of the resonant light is also essential. While circularly polarized light can be generated at synchrotron x-ray sources, it requires specially designed undulators (beamline insertion devices) which means that there are limited numbers of these

beamlines and thus it is harder to gain access. In previous decades, this kind of polarization control was not accessible outside of a few synchrotron light sources. However, recent achievements in nonlinear optics has enabled polarization-controllable soft x-ray/EUV light sources that fit on a standard optical table [6]. These sources produce beams with high spatial coherence, making them good candidates for coherent diffractive imaging, but struggle to produce photon energies above 200 eV or wavelengths shorter than 16.12 nm [7]. Fortunately, the iron M-edge transitions exhibit magnetic circular dichroism effects at about 52.7 eV or 23.5 nm, a photon energy that is much more accessible to High Harmonic Generation (HHG) systems.

# Chapter 2

# Methods

## 2.1 Ptychographic CDI

I will present a brief overview on ptychographic imaging, though J. Miao et al. give an apt introduction to the subject in their review paper [4]. Ptychography is a form of coherent diffractive imaging that uses diffraction patterns produced from several overlapping regions to reproduce an image. Rather than reproducing an image from a single large scan where the beam is larger than the sample and the diffracted and undiffracted portions interfere, ptychography takes several scans and retrieves phase information by using the constraint provided by the regions' overlap. This allows ptychography to reproduce objects much larger than the beam, in fact, given a sufficiently stable beam, stages, and detector, ptychography can reconstruct objects of infinite size.

Ptychographic data is collected as a sample is shifted relative to a beam. In most cases, the sample moves on translational stages in the path of the beam, but occasionally the beam is expanded to the size of the sample and a pinhole or zone plate is moved in front of the beam on translational stages. The light is diffracts as it passes through (or sometimes

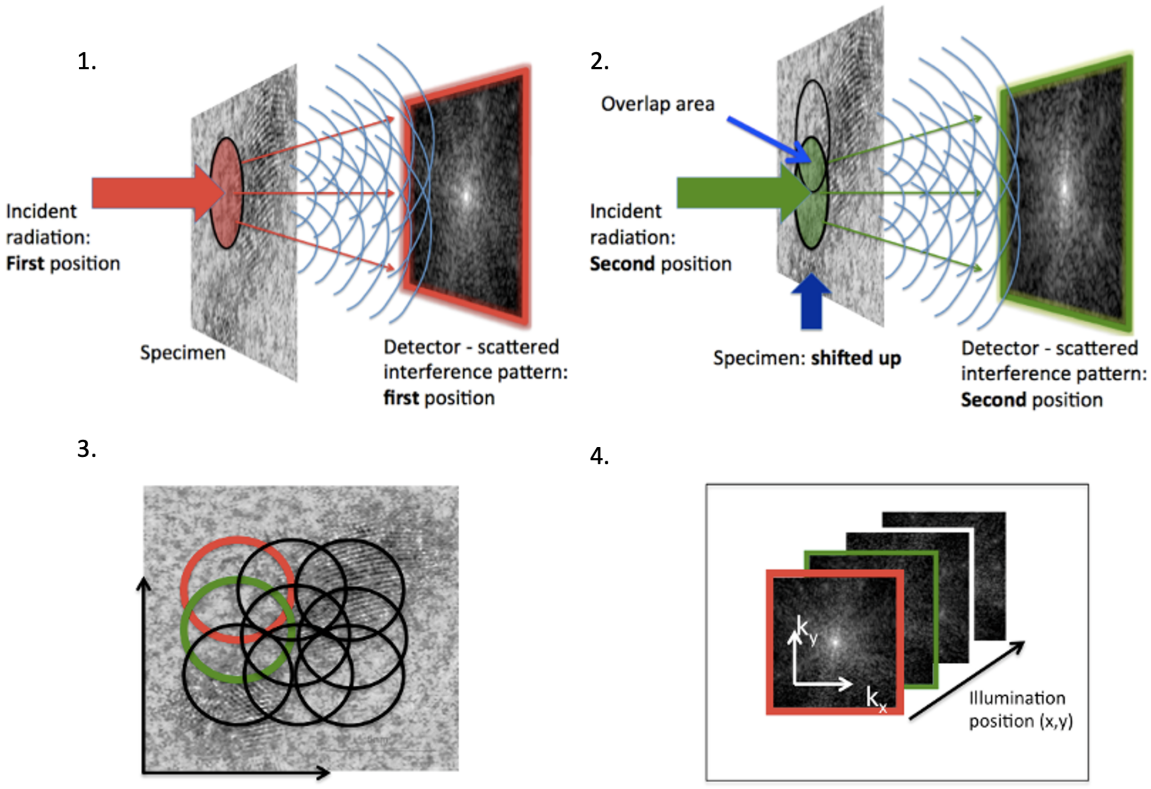


**Figure 2.1** A pictorial explanation of ptychography. The four sub-images are as follows: (1) The beam illuminates a specimen is diffracted by the features thereon, creating a pattern detected on a CCD. (2) A second diffraction pattern is produced from a region that overlaps with the first. (3) More overlapping regions are illuminated, scanning the entire region of interest on the sample. (4) The diffraction patterns and their corresponding positions on the sample are recorded for reconstruction. Modified from [8].

reflects off) the sample and a CCD detector measures the resulting diffraction pattern. As experimentalists scan multiple adjacent and overlapping areas, the dataset collects diffraction patterns and corresponding sample positions. This dataset contains an enormous amount of information regarding the object being imaged, and clever algorithms are required to tease out the image's features from its diffraction patterns.

## 2.2 Two Experimental Setups

While ptychography can be robust in its reconstructions, its performance can be dramatically affected by a number of experimental and computational variations. In order to isolate issues in our ptychographic pipeline, we used two systems—one reliable system capable of relatively low resolution (the helium-neon laser setup) and one more complicated (the high harmonics generation) system capable of much greater resolution. Our goal was to resolve as many issues as possible with our ptychographic techniques on the simpler setup and then apply the polished techniques to our more complex system.

### 2.2.1 Helium-Neon Laser Setup

The first setup employs a Helium-Neon Laser (He-Ne) as its light source (see **Fig.2.2**), as it produces a reliable beam that is visible making it useful outside of vacuum, and not prone to significant thermal drift. This setup reflects a continuous wave 632.8 nm beam off two aligning mirrors before directing it toward the sample and the detector. Then a pinhole and iris increase the spatial coherence of the beam by first creating an airy pattern from the initial beam and then blocking all but the central disc of that pattern. Following the pinhole and iris, a lens was used to make the beam smaller at the sample, thus allowing for greater photon intensities at the point of the probe hitting the sample. In ptychography, the probe is defined

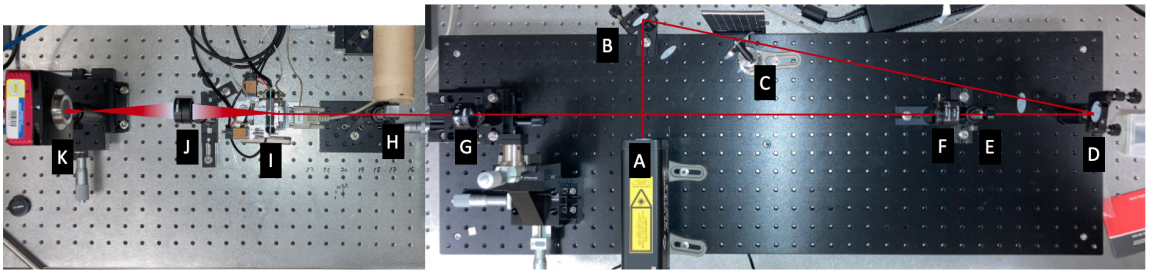


**Figure 2.2** Tabletop Helium-Neon (He-Ne) laser setup. (A) is the He-Ne laser. Beam reflects off mirror (B) then is attenuated by variable attenuator wheel (C). Beam then reflects off mirror (D) and passes through pinhole (E) and order sorting aperture (F). Then the beam passes through focusing lens (G) and passes through beam splitter (H) (H is for other experiments). Finally, the beam, now near its focus, diffracts off sample (I) mounted on horizontal and vertical translational stages. The diffraction pattern passes through lens (J), which brings the far-field diffraction pattern close enough to detect on CCD detector (K) (Thorlabs S805MU1 CCD Camera) while still keeping (K) on the table. As the He-Ne setup is to test ptychographic processes and not the experimental end goal, lenses are permissible. However, on the HHG setup, there are no lenses as explained above.

as the cross section of the beam that hits the plane of the sample, and can be described by the intensity and phase of the beam at that location. These two pieces of information describe all that there is to know about the beam, including its converging or diverging nature and any irregularities, so the reconstruction does not require explicit knowledge of those aspects of the experimental geometry to be successful. The beam diffracts off a specific region of the sample—a region that changes with each new scan. The portion of the diffracted light that continues onward hits another focusing optic, this time bringing the far-field diffraction pattern closer for convenience.

The keen reader will notice that though this setup is for "lensless imaging", it contains two lenses, one for focusing the beam down onto the sample and another just before the camera. The camera would otherwise pick up the near field diffraction pattern, which, to be clear, can be used to reconstruct the object, though with much greater difficulty. These lenses are allowable because this setup is intended to demonstrate ptychographic techniques for use

in imaging with much shorter wavelengths, and these shorter wavelengths produce far-field diffraction patterns at much shorter distances than the 632 nm He-Ne beam. Therefore, this final focusing optic would be unnecessary with the EUV beam.

### 2.2.2 Extreme Ultraviolet Setup

In describing the beam that diffracts off our sample, we must first describe how it was produced. Our setup begins with an ultrafast infrared pulse (duration < 50 femtoseconds) centered at 800 nm in wavelength. This short pulse requires a large bandwidth of composite frequencies, so the pulse, though centered at 800mm, contains wavelengths from 760 to 830 nm. This ultrashort pulse reflects off a few mirrors before it is focused by an anti-reflective coated 1500 mm focusing lens, whose focal length is chosen to put the focus of the beam at the center of the gas cell. The beam, now converging, passes through a fused silica window, entering the vacuum chamber where the harmonics will be generated. This window will cause dispersion and lengthen the pulse, but the laser is tuned to pre-compensate for this. As the beam nears its focus, it passes through a hole in a thin molybdenum sheet that defines the near side of the gas cell. The hole in this sheet is created by the beam and therefore is only as large as is necessary for the brightest part of the beam to pass through. Inside the gas cell (measuring 15mm across and filled with argon at 20 Torr), the beam comes to its focus, generating harmonics that range from 3 to 70 eV. Now the beam contains both the fundamental IR wavelengths and the high harmonics. This spectrum of wavelengths exits the far side of the gas cell through a hole in a molybdenum sheet similar to the one that formed the entrance, and continues downstream.

At this point, the beam has a number of qualities that make it undesirable for imaging. First, the beam is not monochromatic, as it contains both the fundamental IR pulse and the harmonics. As our end goal is to image magnetic materials at a specific photon energy (52.7

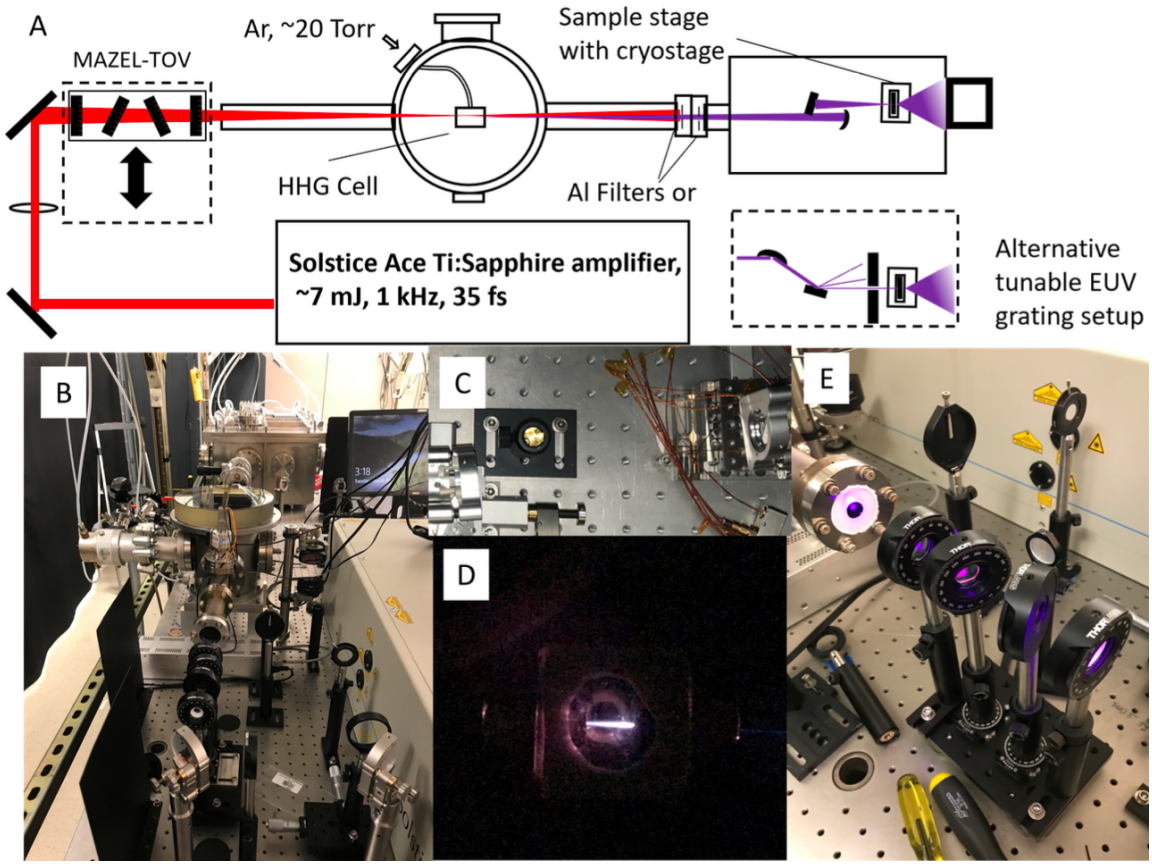


**Figure 2.3** (A) Design of the tabletop EUV source for magnetic imaging, consisting of a Solstice Ace Ti:sapphire amplifier, MAZEL-TOV apparatus, a vacuum system, argon gas cell, and two separate optical designs for selecting harmonics.(B) An image of the tabletop source. (C) An image of the EUV normal-incidence mirror design for selecting a harmonic. (D) The IR beam is focused into a gas cell containing argon gas around 20 Torr pressure where the high harmonics are generated. The IR beam is blocked by two aluminum filters placed in series. The EUV beam transfers through the aluminum filters. The desired harmonic is selected either by normal-incidence EUV mirrors or a toroidal mirror and grating pair. The selected harmonic is then used to probe the sample. (E) The system also contains the insertable MAZEL-TOV apparatus. This allows full polarization tunability between linear and circular polarization. It is important to note that the MAZEL-TOV may not work with the tunable spectrometer since the EUV beam will be at grazing incidence for each optic. This can alter the polarization of the beam. Taken with permission from [6]

eV), the beam must contain only the 52.7 eV harmonic and none of the IR beam. Second, it is diverging: as it exits the gas cell, we can expect it to achieve its previous diameter in 1500 mm and continue growing afterward. The HHG beam will have smaller divergence, as it was generated only in the most intense part of the beam (i.e. the center), but is still diverging, making its intensity much lower than we desire.

The optics immediately downstream help to reduce the first problem by reflecting the beam off two IR beam rejectors (KMLabs Arterium Rejectors) at 7 degrees from grazing incidence. This angle was selected to maximize the ratio of the IR beam absorbed to HHG beam absorbed. After these two reflections off silicon coated mirrors, the beam contains only 5% of the initial IR and up to 95% of the HHG beam directly upstream [9]. After that, a two aluminum filters serve to further reduce the transmission of the IR, while allowing a certain range of harmonics through [10]. While the transmission of the desired photon energies is far less than 1, the IR beam is practically undetectable after two filters each of 100 nm in thickness.

These beam rejectors and thin metal filters greatly reduce the first problem listed, though the beam is still poly-chromatic (it contains more than one harmonic), and it is still diverging. The next set of optics solve both of these problems. After the beam enters the large vacuum chamber, it hits a pair of multilayer mirrors tuned specifically to the wavelength 52.7 eV photons. The first of these mirrors is curved and has a focal length of 25 cm and the second is flat. These mirrors, with their selective reflectivity and focusing geometry, leave the beam ready for imaging, and produce a beam waist as small as 10 microns in diameter. As ptychography depends upon getting sufficient photon flux through the specified part of the sample, this tightly focused beam is crucial.

After the multilayer mirrors, the now monochromatic beam hits the sample, positioned by a set of Attocube stages that move the sample vertically and horizontally in the path

of the beam, allowing it to hit any desired location on the sample. Ptychography data sets consist of diffraction patterns with their corresponding sample positions, so reconstruction resolution is in part limited by the accuracy and precision of these stages.

Finally, the now diffracted beam lands on the CCD detector of the Andor Ikon-L positioned 20 cm away from the sample. In contrast to the He-Ne setup described above, no lens is necessary to bring the detector into the far field, due to the much shorter wavelength being used. In fact, no lens could be used for the EUV beam the way the final lens was used in the He-Ne setup.

## 2.3 Computational Methods

Any type of coherent diffractive imaging is limited in resolution by the geometry of the system and by the relative accuracy of the equipment involved. Both the He-Ne and HHG setups required certain pre-processing techniques before their data sets were ready for reconstruction. First, both CCD detectors are subject to electronic noise in their pixels, meaning that they will register non-zero intensities for pixels that are not touched by the diffracted beam. To some degree this noise can be predicted and its effect subtracted away. We perform this background subtraction–as it is commonly called in the field–by taking a series of dark images whose exposure times add up to the exposures used in the experiment. With the laser blocked or turned off, we can determine just how much of the CCD's reading is due to ambient light, electronic noise, or irregularities in the detector, and then subtract the pixel values of these summed background images from the corresponding pixels from each ptychography frame. It is best to take these images right before the ptychographic data set is taken to ensure that the conditions are as close as possible to the experimental ones.

Occasionally, background subtraction lowers the value of a pixel to below zero, asserting that less than zero photons hit that frame. This type of error can be corrected by another pre-processing noise reduction technique called thresholding. Thresholding involves setting every pixel value below a specified threshold value to zero. Like background subtraction, this method removes detected intensity that is unlikely to result from the beam. Unlike background subtraction, thresholding does so indiscriminately, and thus fails to take into account the few pixels that may be especially "hot," or produce a higher reading than their neighbors whether or not they are detecting a beam. However, when a background subtraction removes more counts from a pixel than were present in the scan, thresholding sets that value to zero, resolving our non-physical reading.

Additionally, the detector can warm over the course of the ptychographic scan, increasing the level of electronic noise more for frames that come later in the set. In data sets with this irregularity, background subtraction with a background taken at the beginning of the scan does not sufficiently lower the noise of the later scans, and a threshold value that appropriately removed all but the actual diffraction peaks in the first scan will allow most of the noise through in the later frames. To resolve this issue, we implemented a variable threshold function in python. This function sorted pixel values from lowest to highest, and then determined what value constituted the percentile specified by the user, setting any pixel value below that threshold to zero. This simple solution can prove quite helpful in many cases, but by removing the bottom 95 percent of pixels on every frame one asserts to some degree that every scan position produces similar net transmission, which may be true for some samples and false for others. Therefore, researchers should recognize this implication and perform thresholding with discretion.

In the He-Ne data set, we discovered another source of noise—the Thorlabs S805MU1 CCD Camera we used produced a vertical bleed artifact. In many of the scans with the

brightest pixels, the ones where most of the beam passed through undiffracted, the pixels in the same column as these brightest pixels also had an elevated value. The charge accumulated in these pixels affected the reading of the pixels below and below them as they were shifted away, thus altering the collected diffraction pattern. Ideally the beam would be attenuated to the point where this effect disappears, or a shutter would be installed to limit the exposure time, but with an otherwise good data set we decided to employ another computational correction to this vertical pixel bleeding. In python, a function was written that performed a type of percentile thresholding for each of the pixel columns that were affected by this vertical bleed. As with all saturation effects, once pixels in the detector register values close to their maximum value of counts, they can no longer be trusted to scale counts linearly with the light incident on them. Additionally, when readings are at this level experimentalists can no longer trust that the charge associated with the reading of the diffraction peaks will not spread to nearby pixels, as seen with this vertical bleed phenomenon. The vertical bleed function helped remove some of these effects, but not all of them.

# Chapter 3

# Results

In this chapter we present results on the ptychographic reconstructions of the data set acquired with the He-Ne laser setup and with the High Harmonic Generation system.

## 3.1 He-Ne Laser Results

We successfully reconstructed several objects with the He-Ne source. These include two test patterns and a wasp wing. We attribute the clarity of the reconstruction to the high signal to noise ratio of the scans and the stability of the beam. On the computational end, there were significant differences between the reconstruction of the scans. All of the reconstructions shown in this section are from the same dataset, though the computational parameters used in the reconstructions varied between the different programs. The sample being imaged was an Air Force resolution test target at 9 lines per mm (see**Fig. 3.1**).


**Figure 3.1** The US Air Force resolution test chart as imaged with a visible light microscope with back-lighting. The number "9.0" here represents 9 lines per millimeter, and the five lines visible at the bottom left are the lines belonging to the 10 lines per millimeter pattern below. There is slight distortion along the edges due to spherical aberration of the lens, but the lines on the sample are indeed straight. The pattern was printed with gold on a glass slide.

### 3.1.1 He-Ne Reconstruction with Ptychodactyl

All data sets were taken with Ptychodactyl, a program written by Nicholas Porter from our lab group. This program can also perform ptychographic reconstructions with the data sets that it acquires, and with the He-Ne scans, these reconstructions were quite successful (see **Fig. 3.2**).

### 3.1.2 He-Ne Reconstruction with Tike

Tike was produced by the Advanced Photon Source at Argonne National Laboratory, and has many of the same optimizations that PyNX does. It supports orthogonalized probe optimization, and performs optimizations for each position instead of performing a single optimization for the entire dataset. PyNX does the latter, making it less useful for reconstructing with a probe that varies from frame to frame (both HHG and x-ray free electron

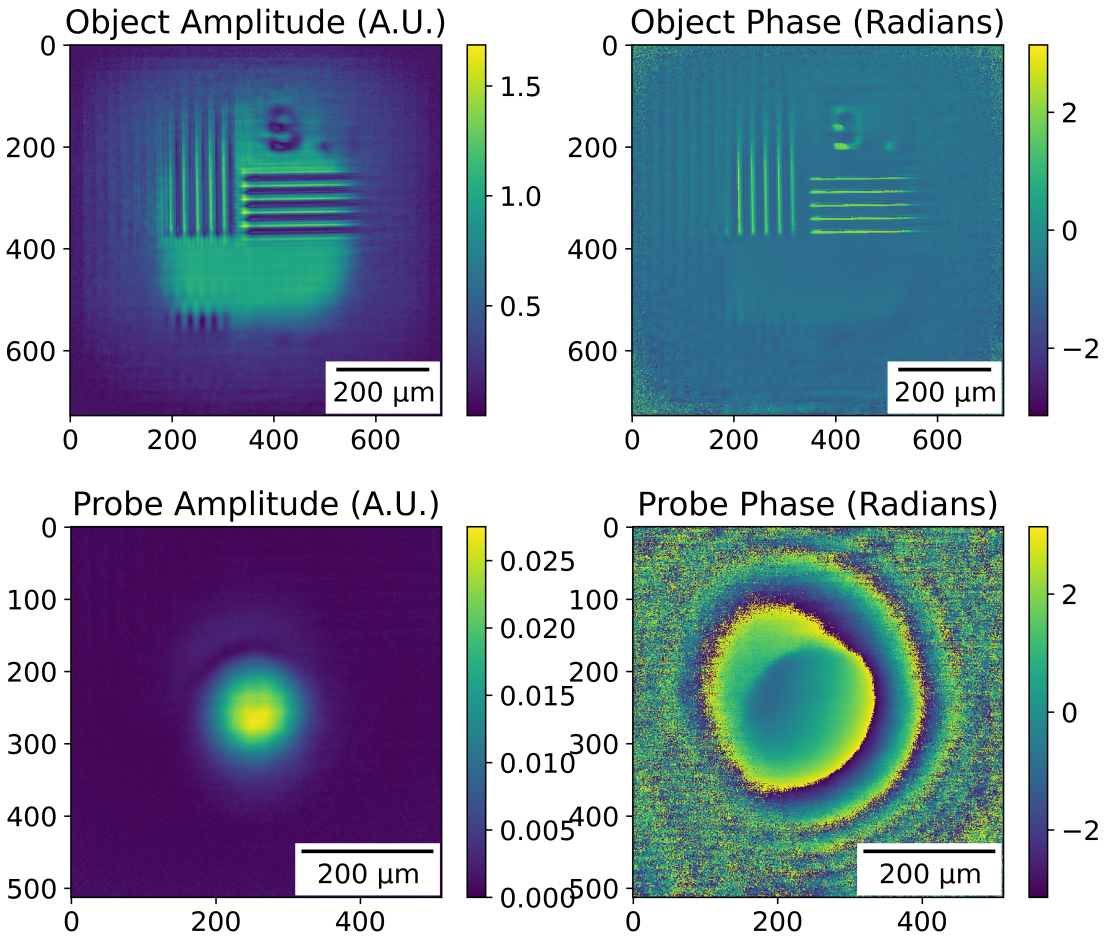


**Figure 3.2** Ptychographic reconstruction of the He-Ne dataset using Ptychodactyl. The upper-left (amplitude) plot contains object information, as expected, but the upper-right (phase) plot contains very similar information, albeit with slightly less clarity. As ptychography reconstructs the exit surface wave, or the phase and amplitude of the beam directly after it interacts with the sample, a retardation in the phase front where the sample contains printed features would be expected. The probe amplitude looks quite neat, with very few features outside the central region of an airy disk other than slight illumination in a semicircle to the upper left of the center. As the phase of the probe shows a phase front centered on the upper left region of the probe, it is probable that the probe was being clipped by the iris upstream, or that one of the lenses was imperfectly aligned.

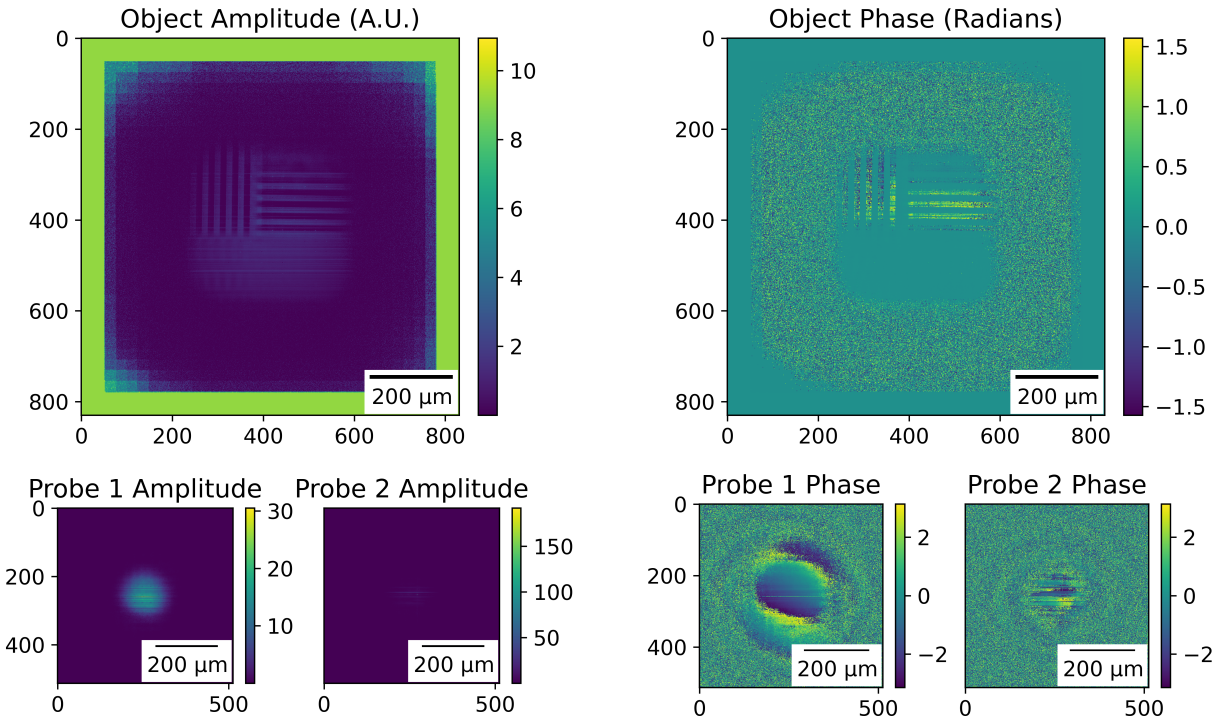


**Figure 3.3** Reconstruction of He-Ne dataset with Tike. This reconstruction was done with two eigenprobes, the first of which looks similar to the Ptychodactyl reconstruction, while the second is a horizontal bar of intensity. The phase information of the reconstruction aligns with the amplitude without providing any new details to the reconstruction. The first probe's phase similar to that of Ptychodactyl's reconstruction. Note the increase in the number of pixels due to padding along the outside of the array.

lasers have this property). Overall, the reconstructions were quite good with this program (see **Fig. 3.3**).

### 3.1.3 He-Ne Reconstruction with PyNX

The European Synchrotron Radiation Facility produced a ptychography code called PyNX, the Python Nanostructures X-tallography toolkit. This open source program is available for download and includes a number of useful features that merited its use as a ptychog-

raphy program. A few of these features were orthogonal probe optimization and position refinement.

Orthogonal probe optimization demonstrates promise as a ptychographic optimization. This probe orthogonalization decomposes the probe into distinct modes that can be weighted individually to compensate for probe shapes that are not necessarily Gaussian.

Position refinement relates to the set of object stage positions that relate to the individual diffraction patterns. If there is instability or irregularity in the in the stage positioning, the recorded diffraction pattern may not sensibly correlate with the overlapping patterns from the neighboring regions. This position refinement option allows the program to adjust the positions in small increments after the fact to find minima in errors between the overlapping positions.

In theory, these two computational techniques should make PyNX a suitable program to process the data from both the HHG system and the He-Ne setup. In practice, PyNX was generally the least successful of all our ptychography programs. As can be seen in **Fig. 3.4**, PyNX produced plots with serious defects from the dataset taken on the He-Ne setup.

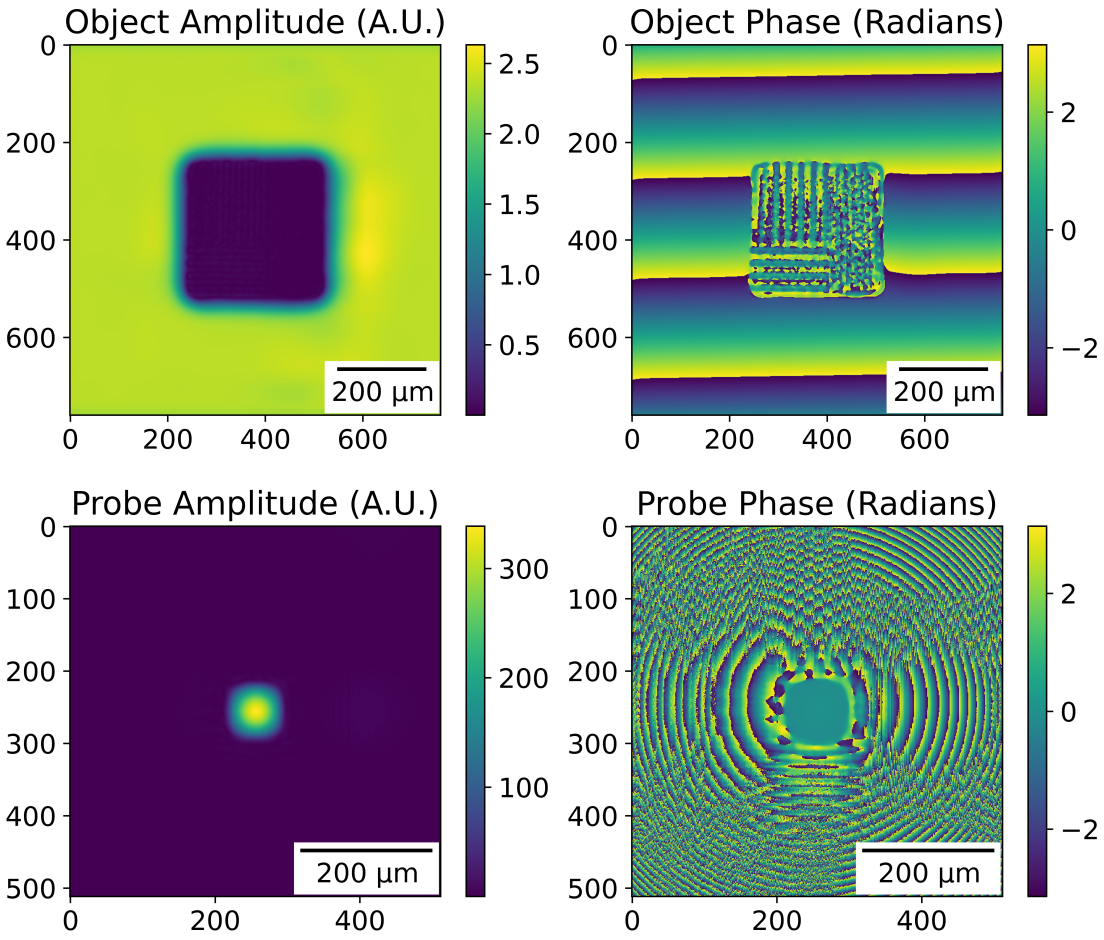


**Figure 3.4** Ptychographic reconstruction of the He-Ne dataset using PyNX. The axes of each plot are pixel numbers, with bar for scale. The upper-left plot shows very little information in the region of interest. The upper-right plot has some of the fringe features expected on the object, but contains additional, erroneous fringes further left. The object appears to be rotated from the other reconstructions, and is missing the "9.0" feature entirely. Additionally, the number of vertical fringes should be 5, and these reconstructions show at least 6. The reconstructions also show a lot of noise.There is a phase ramp from top to bottom, but other reconstructions from this same batch had phase ramp along other axes. Physically, the phase-ramp meaning that PyNX reconstructed a sample with a linearly varying thickness, though the sample has no such linear thickness variation. The bottom-left plot shows the reconstructed probe with a squared-off shape, indicating some rotation or reversal about an axis. The bottom-right plot shows some of the object's features in the phase of the probe, another sign of a failed reconstruction.

## 3.2 High Harmonic Generation Beam Results

While two of the ptychography programs (Tike and Ptychodactyl) performed well with several datasets from the He-Ne setup, the datasets from the HHG system was much more difficult to reconstruct. Eventually, we reconstructed a dataset from the HHG system with Tike, and attempted to reconstruct the same dataset with PyNX with poor results. No attempt was made to reconstruct this dataset with Ptychodactyl.

The sample being imaged with the HHG system was a Y-shaped aperture about 23 by 28 microns (see **Fig. 3.5**). The Y has a pinhole 45 microns from its top, but based on our measurements of the beam this feature should receive very little intensity during the scan, and can thus be ignored. After being used for several ptychography scans, a second light microscope image showed that the aperture had become partly blocked with debris, so it is possible that the reconstructions reflect that to some degree.

We attempted reconstruction with several datasets, many of which varied greatly in their acquisition parameters. A good reconstruction requires dependable data, and so a poor reconstruction is the composite result of the scan acquired and the implementation of the ptychographic reconstruction that follows. Especially with the HHG system, a reliable dataset is not a given. As with the reconstructions in the previous section, all of the reconstructions in this section are of the same dataset, placing the ptychography programs on equal ground for comparison.

### 3.2.1 HHG Reconstruction with Tike

As it did with the dataset from the He-Ne setup, Tike performed quite well with the HHG data. Here it reconstructs a small, but definite Y shape, performing best when given

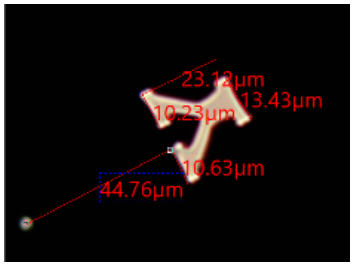


**Figure 3.5** Block Y-shaped aperture cut in anodized aluminum for imaging with HHG system.

orthogonalized probe modes. The reconstructed object amplitude and phase, as well as the amplitudes and phases of the probes are shown in **Fig. 3.6**.

### 3.2.2 HHG Reconstruction with PyNX

Just as PyNX struggled to reconstruct the data from the He-Ne setup, the dataset from the HHG system proved unsuccessful. While the He-Ne reconstruction showed some of the correct object features, the PyNX reconstructions of the HHG data showed no discernible object features. Numerous parameters were used in several thousand reconstructions, but none were successful. As with the He-Ne dataset, almost all of these failed reconstruction contained a significant phase ramp with the region of interest showing lower intensity than the region surrounding it. As with many ptychography programs, a probe guess is fed into PyNX to begin the reconstruction, but as can be seen in **Fig. 3.7**, the program made seemingly little change to the rectangle-Gaussian probe it was given, demonstrating a failed reconstruction.

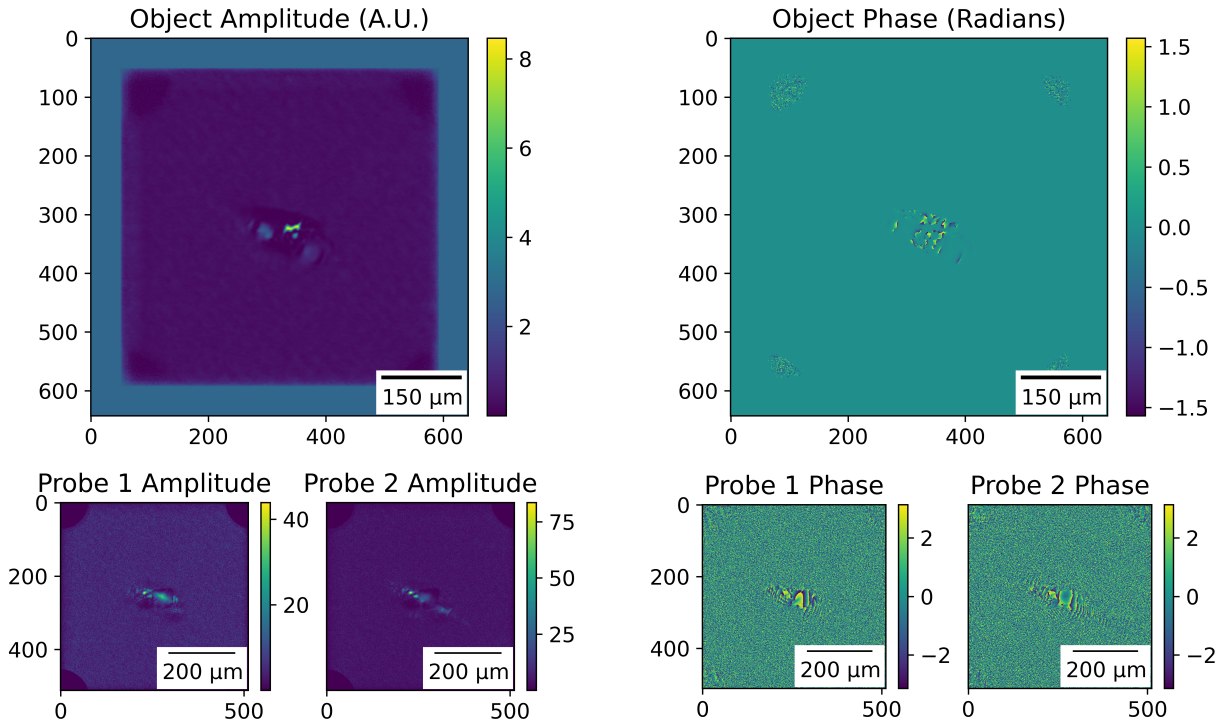


**Figure 3.6** Ptychographic reconstruction of HHG dataset with Tike. This reconstruction was done with two eigenprobes. The Y aperture is small, but clearly visible in the center of the reconstruction. The size of the Y here is due to the geometry of the experimental setup. The object phase appears nonsensical, and in the regions of near zero amplitude, the phase is indeed meaningless. Note the increase in the number of pixels due to padding along the outside of the array, in addition to computational artifacts in the corners of the images.

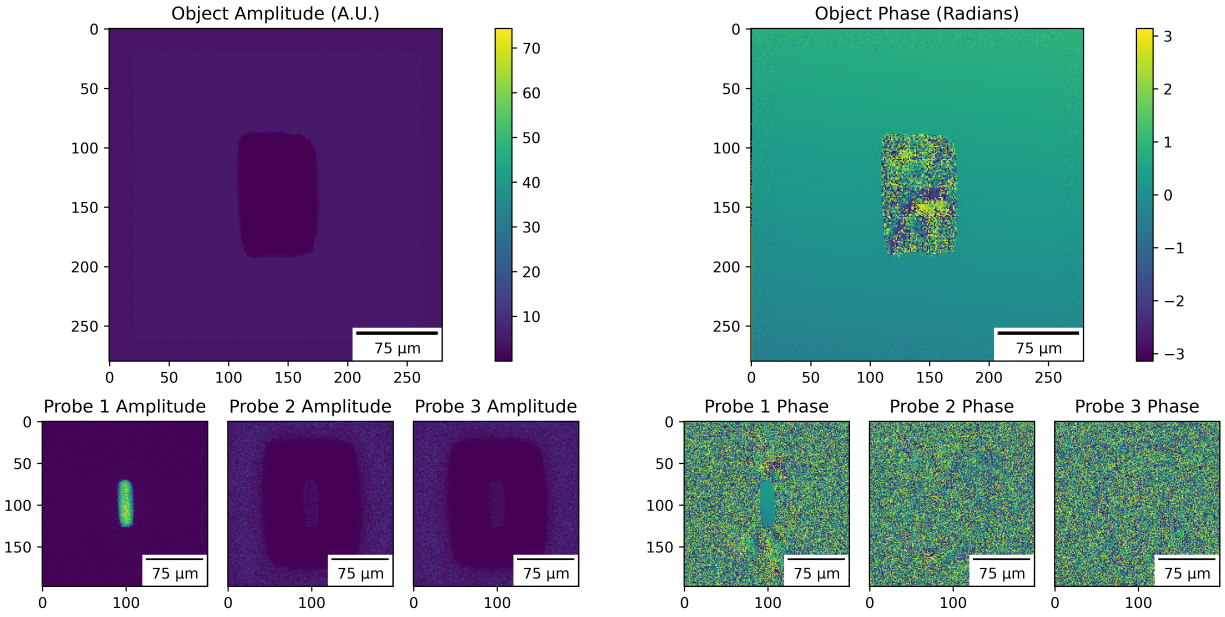


**Figure 3.7** Ptychographic reconstruction of the HHG dataset using PyNX. The axes of each plot are pixel numbers, with bar for scale, just as before. The reconstructed object amplitude shows only a dark patch marking the area swept out by the probe. As seen in the three eigenprobes, there is no The upper-right plot has some of the fringe features expected on the object, but contains additional, erroneous fringes further left. The object appears to be rotated from the other reconstructions, and is missing the "9.0" feature entirely. Additionally, the number of vertical fringes should be 5, and these reconstructions show at least 6. The reconstructions also show a lot of noise.There is a phase ramp from top to bottom, but other reconstructions from this same batch had phase ramp along other axes. Physically, the phase-ramp meaning that PyNX reconstructed a sample with a linearly varying thickness, though the sample has no such linear thickness variation. The bottom-left plot shows the reconstructed probe with a squared-off shape, indicating some rotation or reversal about an axis. The bottom-right plot shows some of the object's features in the phase of the probe, another sign of a failed reconstruction.

# Chapter 4

# Discussion

In the above results, we demonstrate a robust reconstruction of a ptychographic data set taken with a Helium Neon laser. While PyNX and tike under-performed as compared to a much simpler algorithm, it is very likely that they could produce similar results given all of the right optimizations. Tike was much more successful than PyNX, and was the only program to reconstruct a dataset taken on the HHG system, though we haven't tried Ptychodactyl on that data yet. PyNX can produce great reconstructions with datasets from the x-ray light sources similar to where it was designed, but with the data acquired in this lab it has proven unsuccessful. It is probable that with more optimal reconstruction parameters it would perform better.

The reconstructions with the HHG were generally less successful, with the tike reconstructions showing a smaller and blurrier reconstruction than desired, but the size and resolution in these reconstructions is limited by the geometry of the experimental setup. This setup can and will change, and with the sample placed closer to the detector we expect sharper reconstructions. It is also likely that blurriness in the reconstruction was caused by inconsistencies in the scan. The possible points of failure are many but the essentials are

signal to noise ratio, probe variability, and detector variability, all of which have been issues in the past.

With a High Harmonic source, photons are coherent, but often not plentiful. The numerous steps in removing the IR beam and the undesired harmonics reduce the flux of the 41.85 eV beam (our chosen harmonic) by x from its generation to its focus down onto the sample. The IR beam rejectors leave 95% of the harmonic beam intact, but the two 100nm Al filters each permit only 80% of the beam hitting them to continue on. The pair of Multilayer mirrors collectively reflect 30% of the beam directly preceding them, so in assuring a monochromatic beam we remove 95% of the possible imaging photons. This scarcity of photons lowers the signal to noise ratio, making the diffraction peaks harder to see amid the electronic and thermal noise of the detector.

This complicated multi-step process that produces our harmonics is also likely to blame for the probe variability. For over a year, the scans on this system routinely took 2-4 hours, with numerous accumulations per position. These accumulations were expected to average out short term oscillations and inconsistencies in the beam, but the length of the scan made the long term beam inconsistencies a much more relevant factor. The beam can change noticeably from one exposure to the next, but over the course of a few hours it experiences significant drift. Over this time, the Ti:Sapphire laser may change in output power, significantly affecting the HHG beam produced [6]. Also, the beam may widen or change the shape of the holes on the sides of the gas cell, affecting the shape of the IR beam and the harmonics it generates.

Additionally, the CCD detector's cooling system has allowed for enough temperature variation in past scans to produce much more noise in later frames than in earlier ones. While we can apply computational techniques to flatten this effect, the inevitable consequence is that the signal to noise ratio is variable throughout the scan. In the resulting reconstructions,

we expect that the later scans will incorporate more random noise in the reconstructed object at the later positions.

All of these factors become much less relevant with shorter scan times, and by dramatically reducing the number of accumulations, as well as binning with the camera hardware before readout has allowed for scans lasting 3-10 minutes. Over this shorter time scale, the variations in the laser power, gas-cell aperture shape, and camera temperature are negligible, and while there are shifts in the beam from one exposure to the next, these have proven much less harmful to the reconstructions than the long-term changes that these shorter scans avoid. After making these changes to the scan procedure the reconstructions from the HHG system have been much more successful.

There are a few possible changes that would improve the signal to noise ratio and stability of the acquired data. By using one Al filter were used instead of two, the EUV beam would be 25% brighter [10]. The IR beam rejectors are a recent addition to the experimental setup, and before their inclusion the two Al filters were the first line of defense against the IR beam. In this previous setup we were more concerned with the IR beam damaging the filters and subsequently landing on the detector they protect, but with the beam rejectors in place, we can safely remove one of the 100 nm Al filters from the path of the beam. The program that acquires the data (also ptychodactyl) was recently modified to close the shutter and abort the scan if the CCD detector begins to saturate, thus the software acts as a secondary protection for the detector.

Also, the flat multi-layer mirror may be removed and the setup reconfigured; this change alone results in a 69% improvement over current photon counts. However, this would require that the detector be mounted in the chamber, rendering this change quite laborious. Additionally, the pair of mirrors together remove the unwanted harmonics from the beam,

and setups with a single multilayer mirror often have to use more sophisticated ptychography techniques to account for multiple wavelengths in the diffraction patterns [11].

One option for increasing beam stability is including a pinhole directly before the sample. This pinhole would reduce the flux of the probe, but would provide it with more structure and stability. As ptychography is built on the notion that the probe stays more or less constant from one exposure to the next, this modification could significantly improve the reconstructions, but the reduction in the probe intensity would decrease the signal to noise ratio.

With all of these modifications there are trade offs, but in search of further improvements to our reconstructions we may investigate these options.

# Chapter 5

# Conclusion

In conclusion, the Helium-Neon laser ptychographic reconstructions were successful with two of the ptychography programs, Tike and Ptychodactyl, and Tike successfully reconstructed an image with data from the High Harmonic Generation setup. Ptychodactyl provided the most precise reconstructions with the He-Ne data, with Tike showing the features perhaps half as well on the same reconstructions, but with other He-Ne datasets not shown here, Tike has demonstrated excellent reconstruction, suggesting that by optimizing a few reconstruction parameters it may perform at least as well as Ptychodactyl. It is also possible that PyNX could perform similarly given a more optimized recipe, but with all of its options it has proven too complicated to be useful with our reconstructions.

The Y-aperture imaged with Tike is about 25 microns square, but the eventual resolution goal is around 50 nm (assuming a sample to detector distance of between 2 and 3 cm). The images produced in this work are a step in the right direction, but significant improvements will be needed to enable imaging objects in the 30-100 nm range. Because the HHG source is tunable to the Fe-M absorption edge, we conclude that magnetic imaging with this source is possible, but that it will require a level of precision not yet demonstrated here. The

progress reflected in this thesis will help direct our future efforts and better inform our experimental design and reconstructions as we seek this goal.

# Bibliography


[1] J. Peatross and M. Ware, *Physics of Light and Optics* (Brigham Young University, 2022).

[2] S. Braun, H. Mai, M. Moss, R. Scholz, and A. Leson, "Mo/Si Multilayers with Different Barrier Layers for Applications as Extreme Ultraviolet Mirrors," The Japan Society of Applied Physics (2002).

[3] R. Sandberg, "Closing the Gap to the Diffraction Limit: Near Wavelength Limited Tabletop Soft X-Ray Coherent Diffractive Imaging," (2009).

[4] J. Miao, T. Ishikawa, I. K. Robinson, and M. M. Murnane, "Beyond crystallography: Diffractive imaging using coherent x-ray light sources," Science (2015).

[5] J. Stöhr and H. C. Siegmann, *Magnetism: From Fundamentals to Nanoscale Dynamics* (Springer, 2006).

[6] T. Buckway, "Tabletop Extreme-Ultraviolet Source Using High Harmonic Generation for Polarization Sensitive Imaging," (2022).

[7] C. Ding, W. Xiong, T. Fan, D. D. Hickstein, T. Popmintchev, X. Zhang, M. Walls, M. M. Murnane, and H. C. Kapteyn, "High flux coherent super-continuum soft X-ray

source driven by a single-stage, 10mJ, Ti:sapphire amplifier-pumped OPA," Optics Express (2014).

[8] 22sm22, "Ptychography," https://en.wikipedia.org/wiki/Ptychography (2023).

[9] KM-Labs, "Arterium Rejector Modules," Technical report (2023) .

[10] B. Henke, E. Gullikson, and J. Davis, "X-ray interactions: photoabsorption, scattering, transmission, and reflection at E=50-30000 eV, Z=1-92," Atomic Data and Nuclear Data Tables (1993).

[11] P. Baksh, M. Odstrčil, H. Kim, S. Boden, J. Frey, and W. Brocklesby, "Wide-field broadband extreme ultraviolet transmission ptychography using a high-harmonic source," Optics Letters (2016).